

Absolute step and kink formation energies of Pb derived from step roughening of two-dimensional islands and facets

M. Nowicki, C. Bombis, A. Emundts, and H. P. Bonzel*

Institut für Schichten und Grenzflächen, ISG 3, Forschungszentrum Jülich, D-52425 Jülich, Germany

(Received 15 July 2002; revised manuscript received 9 October 2002; published 6 February 2003)

The shapes of (111) oriented two-dimensional (2D) islands and facets, the latter being part of three-dimensional (3D) crystallites of Pb, were equilibrated at 104–520 K. Island sizes were in the range of 15–90 nm radius, facets typically at 100–270 nm radius. They were imaged by scanning tunneling microscopy to provide the exact outline of the bounding step. Increased step roughening with increasing temperature decreases the radius anisotropy of islands and facets in a consistent manner. Products of island/facet radius times local step curvature versus temperature were obtained experimentally, serving as the basis of absolute step and kink energies at 0 K. They are $f_{1A}(0) = 128.3 \pm 0.3$ meV, $f_{1B}(0) = 115.7 \pm 5.8$ meV, and $\varepsilon_{kA} = 42.5 \pm 1.0$ meV, $\varepsilon_{kB} = 60.6 \pm 1.6$ meV, respectively. The combination of studying small 2D islands (unstable at high temperature) and large 2D facets allows measurements over a very large range of temperatures.

DOI: 10.1103/PhysRevB.67.075405

PACS number(s): 68.35.Md

I. INTRODUCTION

Important surface energetic quantities, such as step, surface, and kink energies, can be obtained from a systematic study of two-dimensional (2D) and three-dimensional (3D) equilibrium crystal shapes (ECS).^{1–7} Observations of the ECS at a single temperature will normally provide relative step and surface energies only. The experimental determination of absolute step free energies, kink energies, and also step interaction energies is difficult and requires considerably more effort. On the other hand, absolute step free energies play an important role in governing surface morphologies as well as kinetic processes associated with shape changes, and, furthermore, they are considered to be the key to absolute surface free energies of well-defined low-index orientations.^{7–9}

Several techniques for obtaining absolute step free energies have recently been reported for a number of metallic systems,^{8,10–14} Si surfaces^{15–19} and TiN.^{20,21} Most of those experiments are based on measuring temperature-dependent shape changes or shape fluctuations of small 2D islands carried out under ultrahigh vacuum (UHV) conditions. In one case, island coarsening kinetics are combined with shape analysis to reach this goal.²⁰ Another approach deals with temperature-dependent shape changes of 2D facets present on 3D equilibrated crystallites.^{5,8,14} The latter technique is capable of providing also a quantitative value of the surface free energy of the facet.⁹

Facets on the 3D ECS are at the same time 2D equilibrium shapes whose temperature dependence can be studied and evaluated in the same manner as that of 2D islands on a flat substrate.⁵ Since the facet is in equilibrium with the bulk of the whole crystallite, the size of the facet (i.e., its mean radius) is a direct measure of the step free energy, provided the 3D ECS is regular and differentiable at each point.⁸ In this case, there are two different experiments that can be run to yield absolute step free energies: either a measurement of the facet radius as a function of temperature (of the same crystal⁸) or a measurement of the anisotropic facet shape as a

function of temperature.^{11,12,14,16} In the latter case the changing anisotropy of the step free energy and its theoretical description play a crucial role for the evaluation. A corresponding experiment has already been carried out for (111) facets of 3D Pb crystallites.¹⁴ The current study aims at complementing this previous work by analyzing 2D islands of Pb on large (111) oriented terraces of a thin epitaxial film of Pb on Ru(001), for the following reasons: First, these 2D islands are considerably smaller than the (111) facets studied before, such that their 2D equilibrium shapes can be obtained and imaged below room temperature, thus extending the measurable range to about 100 K. Second, comparing the results from 2D islands and the (111) facets of 3D crystallites offers the possibility of checking the self-consistency of both data sets, e.g., with respect to a possible influence of step-step interactions on the shape of facets.

II. EXPERIMENT

All experiments to be described in this paper were carried out in the same ultrahigh vacuum system below 2×10^{-10} mbars. The system was equipped with a variable-temperature scanning tunneling electron microscope (STM; here Omicron VTSTM), a Pb evaporator and, a cylindrical mirror analyzer for Auger electron spectroscopy. The Pb evaporator was calibrated externally by using a film thickness monitor. STM images could be obtained at constant temperatures of 95–800 K, using liquid nitrogen as coolant for $T < 300$ K. 2D Pb islands were prepared²² as follows: A thin Pb film of about 10–30 nm thickness was deposited at 420 K on a clean Ru(001) surface. This layer was annealed at this temperature for 20 h. Its structure was checked by STM and it showed large (111) terraces separated by monatomic steps. To obtain small 2D islands on these terraces, the crystal had to be cooled below 200 K during further Pb deposition. Cooling was accomplished on the STM stage and about 0.1 nm of additional Pb was deposited on the cold surface, yielding mostly 2D islands of monatomic height. A section of such an annealed film with islands imaged at 150 K is shown in Fig. 1(a). Overall, the mean radii were in the range

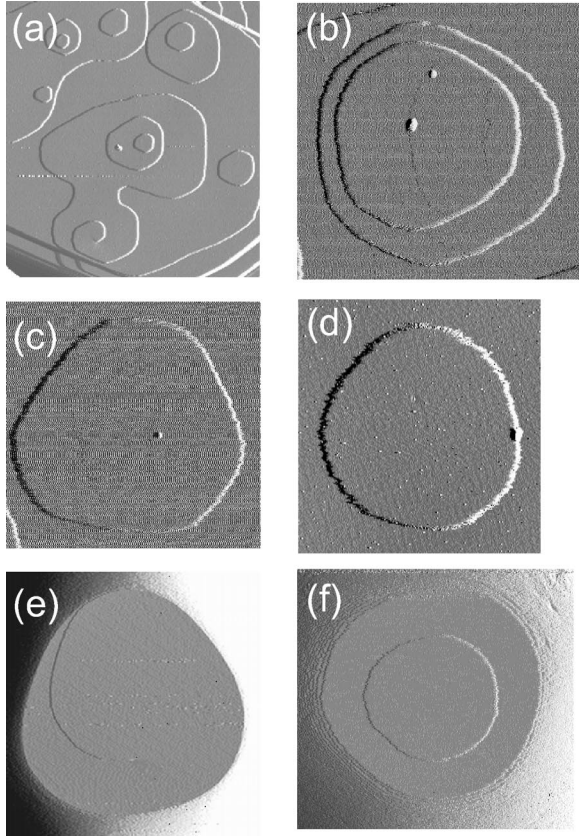


FIG. 1. STM images of 2D islands and Pb(111) facets. (a) Section of flat film with 2D islands at $T=150$ K. Image size: 250×250 nm. (b) Island shape at 167 K, mean radius of upper island at 36 nm. (c) Island shape at 172 K, mean radius at 32 nm. (d) Island shape at 277 K, mean radius at 42 nm. (e) (111) facet shape at 308 K, mean radius at 280 nm. (f) (111) facet shape at 323 K, mean radius at 110 nm. Well resolved monatomic steps outline the facet boundary.

15–90 nm depending on annealing temperature subsequently chosen between 100 and 300 K for shape equilibration. Constant temperature below 300 K was achieved by flowing nitrogen (gas or liquid) through the cryostat connected to a Cu block in contact with the STM sample holder. The temperature, which was measured by a silicon diode on the Cu block, could be selected by adjusting the nitrogen flow rate. Under this condition the thermal drift for STM imaging was minimal. It was assumed that the temperature of the Ru substrate was equal to that of the Cu block within 5 deg.

The preparation of 3D Pb crystallites has been described before.^{23,25,44} In brief, a thin film of Pb, about 20–30 nm thick, was deposited at 300 K on a clean Ru(001) surface. Melting of the film and subsequent freezing generated a distribution of crystallites which were equilibrated at 300–550 K.^{23–25} The (111) facets of the Pb crystallites were imaged by STM at temperatures in a range up to 510 K.²⁶ Imaging at the temperature of equilibration is important for ensuring thermodynamic equilibrium.^{7,27} Although 3D equilibrium may not be fully achieved at room temperature, there is evidence that 2D shape equilibrium of the (111) facets is reached.

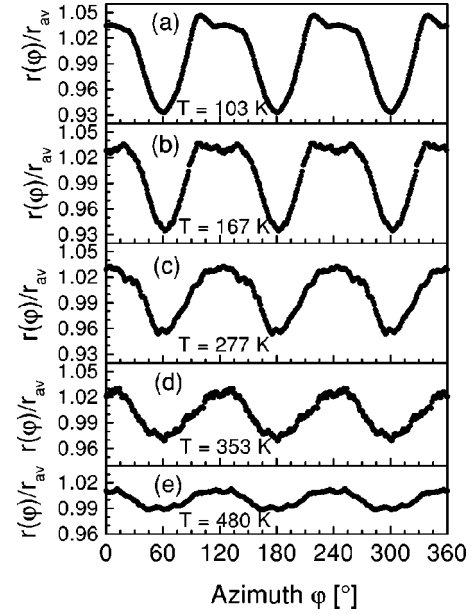


FIG. 2. Cartesian plots of 2D island and (111) facet radii, $r(\varphi)/r_{av}$, threefold averaged and normalized to the mean radius r_{av} , versus azimuth. Data represent five different temperatures: 103, 167, 277, 353, and 480 K. The first three at $T < 300$ K are from 2D islands, the last two from (111) facets of 3D Pb crystallites. Note decrease in anisotropy with increasing T . Minima indicate positions of B steps.

III. RESULTS AND EVALUATION

Figure 1 shows examples of STM images of 2D islands and (111) facets annealed at several temperatures. The threefold symmetry is particularly well seen at lower temperatures of 167–172 K, Figs. 1(b) and 1(c), and corresponds to a maximum radius anisotropy r_A/r_B of about 10%. At 277 K the island shape is much more rounded, Fig. 1(d). Two (111) facet images at 308 and 323 K are shown in Figs. 1(e) and 1(f). The vicinal steps surrounding the facet can be well seen in the latter image. The facet itself exhibits a separate 2D island on top, which essentially has the same shape as the facet. The facet in Fig. 1(e) shows a single step emerging from a dislocation threading the surface. In this case the facet bounding step is even an open loop, but its shape is not different from the equilibrium shape of a nondislocated facet. The temperature-dependent anisotropy of the step free energy, $f_1(\varphi, T)$, which is responsible for the facet symmetry, arises from two inequivalent close-packed steps, with their edges perpendicular to the $[2\bar{1}\bar{1}]$ and $[\bar{2}11]$ (and equivalent) directions.²⁸ These are commonly referred to as A - and B -type steps, respectively. Steps in the intermediate low-index $[\bar{1}10]$ and equivalent directions are fully kinked for geometric reasons (even at 0 K) and have the highest energy. The rather straight sections of the island boundaries in Fig. 1 are due to B steps, which have the lower step free energy.^{24,29}

STM images, as in Fig. 1, provide the database for extracting the outline of the step bounding the island or the facet. Examples are shown in Fig. 2 as Cartesian plots $r(\varphi)$, with r being the radius and φ being the azimuthal angle, after some image distortion in the scanning direction, mostly due

to slow piezo relaxation, has been corrected. The data were also threefold averaged in accordance with the symmetry of the [111] crystal axis. The anisotropy slowly decreases with increasing temperature, illustrated for 103, 167, 277, 353, and 480 K. The anisotropy amounts to about 11% at 103 K and 2.5% at 480 K. The first three plots are data from 2D islands; the latter two from (111) facets.¹⁴ The changing anisotropy is also connected with a concomitant change of the local step curvatures, especially in the directions of *A* and *B* steps—an issue that will become important further below. The advantage of combining the investigation of 2D islands with that of facets on 3D crystallites is that 2D islands of small size can be prepared and equilibrated at low temperature, whereas rather large crystallites and hence facets, resulting from the dewetting/freezing cycle, must be equilibrated at relatively high temperatures (all relative to the absolute melting point of Pb at 600.7 K). Hence the two rather different preparations allow one to cover a large range of temperature.

For a quantitative evaluation of island/facet shapes, the data, such as in Fig. 2, are at first fitted by the function

$$r(\varphi) = r_{av} + \Delta r [\cos(3\varphi + \varphi_0) + H \cos(6\varphi + \varphi_0 + \Delta\varphi)], \quad (1)$$

where $r_{av} = (r_A + r_B)/2$, $\Delta r = (r_A - r_B)/2$, with r_A and r_B as the local radii in the directions of the *A* and *B* steps. The $\cos(3\varphi)$ term is analogous to the $\cos(6\varphi)$ function for 2D hexagonal symmetry shapes.³⁰ Equation (1) has minima at $3\varphi + \varphi_0 = n\pi$ ($n=1,3,\dots$), the position of *B*-step directions. The second term $H\cos(6\varphi + \varphi_0 + \Delta\varphi)$ represents a contribution from the $\langle 110 \rangle$ type steps where $\Delta\varphi = \pi + \varphi_0$ is the phase shift between the two contributions in the bracket. The influence of these steps can be noted in the Cartesian $r(\varphi)$ plots, particularly at low temperature (<400 K), by broader maxima or even extra minima (<250 K) in the region of *A* steps and sharper minima at the *B* steps, as in Fig. 2(b). In general, the fit curves yield a good value of the anisotropy r_A/r_B . Second, when applied to a finite section of $r(\varphi)$, e.g., $\pm 20^\circ$ relative to the direction of *A* or *B* steps, values of the local temperature-dependent curvatures $K_A(T)$ and $K_B(T)$ were obtained. In general, shapes in the vicinity of *A* and *B* steps were fitted as a function of angular range to see whether the curvature would converge to a constant value. However, imaging problems and noise were often too serious to trust an extrapolated or small angle value. Values calculated for ranges of $\pm 10^\circ$ to $\pm 20^\circ$ (relative to the ideal step direction) were averaged and taken to represent the best value of $K_{A,B}(T)$.

The principal data to be extracted from the measured facet shape are the radii r_A and r_B and the corresponding curvatures at the locations of *A* and *B* steps, $K_A(T)$ and $K_B(T)$, where $K(\varphi) = [r(\varphi) - r''(\varphi)]/r^2(\varphi)$ [note that $r'(\varphi) = dr/d\varphi$, $r'(\varphi) = 0$ for the ideal *A* and *B* step directions]. With $r(\varphi)$ given by Eq. (1), the curvatures were calculated. The product of facet radius and curvature, $r(\varphi)K(\varphi)$, is a dimensionless quantity that can be shown to be equal to the ratio of step free energy over step stiffness, $\tilde{f}_1(T)$, for 2D equilibrium forms:^{14,16,31}

$$r_{A,B}(T)K_{A,B}(T) = \frac{f_{1A,B}(T)}{\tilde{f}_{1A,B}(T)}. \quad (2)$$

This relationship follows from the Gibbs-Thomson equation applied to the facet edge on a 3D ECS. The same equation has also been derived for 2D islands by Giesen *et al.*¹² From this, one may conclude that it is valid for 2D islands, irrespective of these being isolated on a flat substrate or facets on a 3D ECS. An important difference is however the temperature dependence of the radius of the 2D entity. The mean radius of a single 2D island may change with time due to Ostwald ripening, especially difficult to avoid at higher temperatures. Disregarding for the moment this undesirable process in the current context of equilibrium shapes, it is clear that the mean radius of an “isolated” 2D island does not depend on temperature, but that of a facet as part of a single 3D equilibrium crystallite does indeed. In fact, its temperature dependence is equal to that of the step free energy. On the other hand, as long as we consider pure shape changes as a function of temperature, 2D islands and facets are analogous, such that we can ignore the temperature dependence of radii. The relationship (2) is expected to be valid for 2D islands and facets, and for *A* and *B* steps. With the product $r_{A,B}K_{A,B}(T)$ being equal to $[1 - r''(\varphi)/r(\varphi)]_{A,B}$, we expect $r_A K_A(T)$ to be <1 at low temperature, where $r_A'' > 0$ due to a small minimum in the direction of *A* steps, but >1 at high temperatures because r_A'' becomes negative. In this range the local radius of the *A* step curvature is smaller than r_A —a feature that is never observed for *B* steps. On the other hand, $r_B K_B(T)$ is always <1 simply because r_B'' is >0 at all temperatures.

The right-hand side of Eq. (2) can be obtained theoretically. The temperature dependence of the step free energy, due to configurational entropy, is given by^{32–34}

$$f_1(T) = f_1(0) - 2kT \exp\left(-\frac{\varepsilon_k}{kT}\right). \quad (3)$$

Here we have neglected vibrational entropy contributions to the step free energy^{8,35–41} but will return to this point later on. Step energies $f_1(0)$ and kink energies ε_k are different for *A* and *B* steps, with the *B* step having the lower step energy and higher kink energy.^{5,14,42} Therefore the less curved part of a (111) facet is indicative of the *B* steps in $[\bar{2}11]$ direction. The step stiffness to first order is given by⁴⁴

$$\tilde{f}_1(T) = \frac{2kT}{3} \exp\left(\frac{\varepsilon_k}{kT}\right), \quad (4)$$

such that we know the ratio $f_1(T)/\tilde{f}_1(T)$ in this degree of approximation. Both of these equations are not expected to be valid for very high temperatures, $T > \varepsilon_k/k$ (Ref. 14). A plot of all experimental values $r_A K_A(T)$ and $r_B K_B(T)$, collected for Pb(111) 2D islands and facets of 3D crystallites, versus temperature is presented in Fig. 3. The data are fitted by first-order functions $f_{1A,B}/\tilde{f}_{1A,B}$. The resulting step energies at 0 K are 115 meV and 127 meV for the *A* and *B* steps, respectively, and corresponding kink energies of 39.7 and 62.8 meV. One can see that the simple first order theory

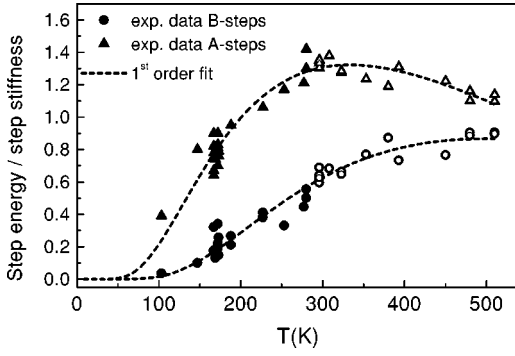


FIG. 3. Plot of experimental data of $r_{A,B}K_{A,B}(T)$ for A and B steps fitted by first-order equations of step free energy over step stiffness versus temperature. Filled symbols are from Pb(111) 2D islands, open symbols from (111) facets (Ref. 14).

describes the experimental data of both A and B steps, although the anisotropy $r_B/r_A = f_{1B}/f_{1A}$ is > 1 instead of the experimentally expected value below 1. One reason is likely to be that Eqs. (3) and (4) are not valid in the high-temperature regime. In particular, the condition $T < \varepsilon_k/k$ is partially violated for A steps because of their low kink energy. Next we used more accurate second-order equations for the step free energy and step stiffness instead of the first-order Eqs. (3) and (4). They were derived from the exact solutions for islands of hexagonal symmetry,⁴³ generated in the framework of the Ising model theory. The second-order expressions follow closely the exact functions for $T < \varepsilon_k/k$ (Ref. 44) and are as follows:

$$f_1(T) = f_1(0) - kT \left\{ 2 \exp\left(-\frac{\varepsilon_k}{kT}\right) - \exp\left(-\frac{2\varepsilon_k}{kT}\right) \right\}, \quad (5)$$

$$\tilde{f}_1(T) = \frac{2kT}{3} \left\{ \exp\left(\frac{\varepsilon_k}{kT}\right) - 4 \exp\left(\frac{2\varepsilon_k}{kT}\right) \right\}. \quad (6)$$

Note, however, that Eq. (5) deviates from the exact form⁴³ by allowing the step energy at $T=0$ K to be independent of the Ising value $f_1^{Ising}(0) = 2\varepsilon_k$. Since the condition $T < \varepsilon_k/k$ is more easily met by B steps than A steps, we at first fit the experimental B -step data to the second-order ratio $f_1(T)/\tilde{f}_1(T)$, shown in Fig. 4. The results are $f_{1B}(0) = 115.7 \pm 5.8$ meV and $\varepsilon_{kB} = 60.6 \pm 1.6$ meV. Because of the good quality of the fit and since $T < \varepsilon_k/k$ is fulfilled, we consider these values for B steps to be reliable. A corresponding fit of the A -step data by the second-order ratio in the low-temperature range up to 280 K yields $f_{1A}(0) = 101 \pm 9$ meV and $\varepsilon_A = 37 \pm 1.6$ meV—both values being even lower than those obtained by the first-order fit in Fig. 3. This behavior indicates that the second-order approximations of the Akutsu expressions are not valid for A steps. The main reason is that the A -step data show ratios of $f_1(T)/\tilde{f}_1(T) > 1$ above 180 K and an asymptotic approach of the ratio of 1 at high temperature. The exact Akutsu equations as well as the second-order approximations with $f_1^{Ising}(0) = 2\varepsilon_k$ do not allow the ratio $f_1(T)/\tilde{f}_1(T)$ to become larger than 1.⁴⁴ On the other hand, by choosing $f_1^{Ising}(0)$ to be independent of

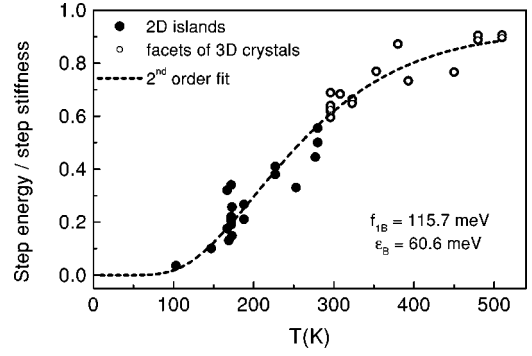


FIG. 4. Experimental data of $r_B K_B(T)$ for B steps versus temperature, fitted by second-order equations derived from the Akutsu equations (4.31) and (4.33) (Ref. 43). The extracted step and kink energies at 0 K are $f_{1B}(0) = 115.7$ meV and $\varepsilon_{kB} = 60.6$ meV. Filled symbols are from Pb(111) 2D islands, open symbols from (111) facets (Ref. 14).

$2\varepsilon_k$, the thus modified equations generate $f_1(T)/\tilde{f}_1(T) > 1$ but diverge at high temperatures. Hence the experimentally determined maximum in $f_1(T)/\tilde{f}_1(T)$ versus T for A steps cannot possibly be fitted by either the exact or the modified Akutsu equations.^{43,44} This is unsatisfactory, especially since we want to utilize as many experimental points as possible for determining correct energies for the A -step.

For that reason the energies for A steps were obtained by fitting the measured anisotropy ratio $f_{1A}(T)/f_{1B}(T)$, keeping the already determined values of $f_{1B}(0)$ and ε_{kB} fixed. The data in Fig. 5 were fitted with the first-order expressions as a simple test, yielding $f_{1A}(0) = 128.0 \pm 0.3$ meV and $\varepsilon_{kA} = 45.0 \pm 0.7$ meV. For comparison, the ratio $f_{1A}(T)/f_{1B}(T)$ was also calculated with the exact Akutsu expressions (except allowing for independent values of $f_1(0) \neq 2\varepsilon_k$). A visual fit of this function to the complete set of experimental data was carried out, using the first-order step and kink en-

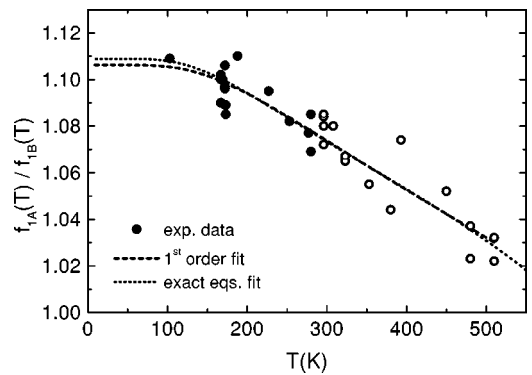


FIG. 5. Ratio of experimental shape anisotropy $r_A(T)/r_B(T)$ versus T , fitted by a theoretical first-order and exact ratio $f_{1A}(T)/f_{1B}(T)$ due to Akutsu *et al.* (Ref. 43), modified to allow independent values of $f_1(0) \neq 2\varepsilon_k$. The values of $f_{1B}(0)$ and ε_k for B steps determined in Fig. 4 were kept constant. The first-order fit yields $f_{1A}(0) = 128.0$ meV and $\varepsilon_{kA} = 45.0$ meV for A steps. The fit with the exact equations yields $f_{1A}(0) = 128.3$ meV and $\varepsilon_{kA} = 42.5$ meV for A steps. Filled symbols are from Pb(111) 2D islands, open symbols from (111) facets (Ref. 14).

TABLE I. Step and kink energies (in meV/atom) for Pb(111) vicinal surfaces, obtained through different evaluation steps explained in the text. Values in bold are considered to be final.

Physical parameter	Evaluation	A step	B step	Energy ratio	Reference
Step energy $f_{1A,B}(0)$	1st order eq., Fig. 3	115±3	127±6	1.125	Present work
	2nd order eq., Fig. 4		115.7±5.8		
	1st order eqs., Fig. 5	128.0±0.3		0.904	
	Exact Akutsu eqs., Fig. 5	128.3±0.3		0.902	
Step energy $f_{1A,B}(0)$	Expt.	131	117	0.893	14
Step energy $f_{1A,B}(0)$	Theory	95	78	0.821	42
Kink energy $\varepsilon_{kA,B}$	1st order eq., Fig. 3	39.7±0.6	62.8±1.5	1.58	Present work
	2nd order eq., Fig. 4		60.6±1.6		
	1st order eqs., Fig. 5	45.0±0.7		1.35	
	Exact Akutsu eqs., Fig. 5	42.5±1.0		1.43	
Kink energy $\varepsilon_{kA,B}$	Expt.	40.0	60.3	1.51	14
Kink energy $\varepsilon_{kA,B}$	Theory	41	60	1.46	42

ergies as starting values. The resulting fit, included in Fig. 5, behaves very much like the first-order ratio. The values obtained are $f_{1A}(0)=128.3\pm 0.3$ meV and $\varepsilon_{kA}=42.5\pm 1.0$ meV, only slightly different from the simple first-order fit. It appears from this general comparison as if the first-order equations have a wide range of applicability for describing the T dependence of $f_{1A}(T)/f_{1B}(T)$.

Overall, it is clear from this multiple-path evaluation of shape anisotropy data that A steps are characterized by a significantly lower kink energy than B steps, consistent with the higher curvature of A steps at elevated temperatures. The corresponding step energies are higher for the A steps at all studied temperatures. The current evaluation leads then to a reasonable description of the anisotropy $r_A/r_B(T)$ and as such confirms earlier results published for facets only.¹⁴ The higher accuracy of energies obtained is believed to come from the extended range of investigated temperatures. At sufficiently low temperatures there is, of course, no difference between the first- and second-order equations. The use of the exact Akutsu equations to fit the ratio $f_{1A}(T)/f_{1B}(T)$ over the whole studied temperature range strengthens the level of reliability of A -step energies. A summary of all energies is given in Table I.

IV. DISCUSSION

The current experimental study of the 2D island shape changes due to step roughening covers the largest relative range of temperature investigated for any material so far. It is the only example in the literature where the ratio of step energy to step stiffness for two kinds of steps has been studied from the realm of exponential increase at low temperatures to the near saturation regime at high temperatures, as summarized in Fig. 3. The overall consistency of the data originating from 2D islands and facets of 3D ECS is quite good, although the level of scatter in the data is still disturbing. The results in terms of the final step and kink energies are in good agreement with those of a previous study¹⁴ and also of theory.⁴² This is especially true for the kink formation energies that seem to be relatively insensitive to experimen-

tal scatter and the path of evaluation.

In our previous discussion, we noted a significant difference in the results to a related study by Arenhold *et al.*⁵ In that work we had attributed the observed Pb(111) facet anisotropy of about 9%, measured at room temperature, to the equilibration temperature of, e.g., 440 K. This resulted in much lower step energies.⁵ It is now clear that the facet as well as the 2D island shapes of Pb can change substantially during cooling.^{7,26,27} Currently we have imaged all 2D island and facet shapes *at* the annealing temperature. Only then do we find a systematic variation of shape anisotropy with temperature, in the sense that it clearly decreases with increasing temperature, despite considerable noise (Figs. 2 and 5).

The role of the step vibrational entropy^{36–39} in the current evaluation of absolute step free energies and kink energies has been dealt with in a previous publication.¹⁴ For the type of steps under consideration, the magnitude of this entropy in harmonic approximation was estimated to be 0.032 meV/K.^{8,14} In short, the relatively small step entropy may be neglected when fitting the experimental data by the theoret-

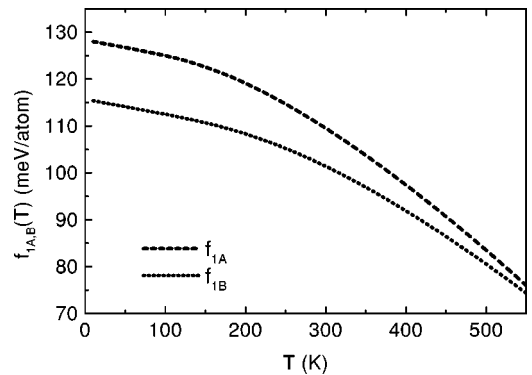


FIG. 6. Plot of step free energies of A and B steps versus temperature, based on the exact equations by Akutsu *et al.* (Ref. 43) modified to allow independent values of $f_1(0) \neq 2\varepsilon_k$ and including a constant vibrational step entropy of 0.032 meV/K (Ref. 8). The input energies are $f_{1A}(0)=128.3$ meV, $\varepsilon_{kA}=42.5$ meV and $f_{1B}(0)=115.7$ meV, $\varepsilon_{kB}=60.6$ meV.

ical ratio function $f_{1B}(T)/\tilde{f}_{1B}(T)$ or by $f_{1A}(T)/f_{1B}(T)$, because it appears in both the numerator and the denominator. On the other hand, for a complete description of the temperature dependence of the step free energy itself, one has to use an appropriate equation that includes the vibrational entropy contributions.^{14,41} We illustrate the temperature dependence of the step free energies of the *A* and *B* steps in Fig. 6 by using the exact Akutsu equations⁴³ and including a constant vibrational entropy for both. The input values are the best-fit step and kink energies of both steps in Table I (shown in bold print). Finally, note that the step vibrational entropy is particularly important in a discussion of the temperature dependence of the step to surface free energy ratio, equal to the geometric ratio of the facet radius to crystal radius on regular 3D ECS.⁹

We conclude the discussion with a brief review of theoretical step energies for Pb(111) vicinal surfaces at 0 K. A recent first-principles calculation reported $f_{1A}(0)=95$ meV and $f_{1B}(0)=78$ meV.⁴² An embedded atom model calculation, based on an interaction potential that duplicates the average Pb surface free energy at 38 meV/Å²,⁴⁵ yielded a step energy of 112 meV averaged over *A* and *B* steps.⁴⁶ In terms of an Ising model, $f_1(0)$ is equal to $2\varepsilon_k$, and when averaged over both types of steps, this would lead to about 100 meV

with the current kink energies. The so-called awning model that relates kink and step energies geometrically,⁴⁷ yields for a step on fcc(111) $f_{1A}(0)=111.3$ meV and $f_{1B}(0)=100.7$ meV, based on the kink energies in Table I. The ratio $f_{1B}(0)/f_{1A}(0)=0.905$ is almost exactly the experimental value.

In conclusion, the systematic study of shape anisotropy of 2D islands and (111) facets of Pb crystallites over a large temperature range of 103–520 K has shown that reliable step and kink energies can be obtained for *A* and *B* steps, and, furthermore, that all data can be consistently described by a single physical model. Hence no recognizable difference in behavior of islands and facets has been found, indicative of a negligible influence of neighboring steps on the facet shape.

ACKNOWLEDGMENTS

We gratefully acknowledge fruitful discussions with and suggestions by Professor Harald Ibach and Professor Paul Wynblatt (Carnegie-Mellon University, Pittsburgh). One of us (H.P.B.) thanks Professor Gerhard Ertl for a sabbatical at the Fritz-Haber-Institut (Berlin), where this paper was actually written.

*Electronic address: h.bonzel@fz-juelich.de

¹J.C. Heyraud and J.J. Métois, Surf. Sci. **128**, 334 (1983).

²J.J. Métois, G.D.T. Spiller, and J.A. Venables, Philos. Mag. A **46**, 1015 (1982).

³J.M. Bermond, J.J. Métois, X. Egéa, and F. Floret, Surf. Sci. **330**, 48 (1995).

⁴Z. Wang and P. Wynblatt, Surf. Sci. **398**, 259 (1998).

⁵K. Arenhold, S. Surnev, H.P. Bonzel, and P. Wynblatt, Surf. Sci. **424**, 271 (1999); **441**, 223(E) (1999).

⁶M. Wortis, in *Chemistry and Physics of Solid Surfaces VII*, edited by R. Vanselow and R. Howe (Springer-Verlag, Berlin, 1988), pp. 367–405.

⁷H.P. Bonzel, Prog. Surf. Sci. **67**, 45 (2001).

⁸H.P. Bonzel and A. Emundts, Phys. Rev. Lett. **84**, 5804 (2000).

⁹Ch. Bombis, A. Emundts, M. Nowicki, and H.P. Bonzel, Surf. Sci. **511**, 83 (2002).

¹⁰D.C. Schlösser, L.K. Verheij, G. Rosenfeld, and G. Comsa, Phys. Rev. Lett. **82**, 3843 (1999).

¹¹G. Schulze Icking-Konert, M. Giesen, and H. Ibach, Phys. Rev. Lett. **83**, 3880 (1999).

¹²M. Giesen, Ch. Steimer, and H. Ibach, Surf. Sci. **471**, 80 (2001).

¹³Ch. Steimer, M. Giesen, L. Verheij, and H. Ibach, Phys. Rev. B **64**, 085416 (2001).

¹⁴A. Emundts, M. Nowicki, and H.P. Bonzel, Surf. Sci. **496**, L35 (2002).

¹⁵B. Swartzentruber, Y.W. Mo, R. Kariotis, M.G. Lagally, and M.B. Webb, Phys. Rev. Lett. **65**, 1913 (1990).

¹⁶N.C. Bartelt, R.M. Tromp, and E.D. Williams, Phys. Rev. Lett. **73**, 1656 (1994).

¹⁷N.C. Bartelt and R.M. Tromp, Phys. Rev. B **54**, 11 731 (1996).

¹⁸H.J.W. Zandvliet, H.B. Elswijk, E.J. van Loenen, and D. Dijkkamp, Phys. Rev. B **45**, 5965 (1992).

¹⁹H.J.W. Zandvliet, S. van Dijken, and B. Poelsema, Phys. Rev. B **53**, 15 429 (1996).

²⁰S. Kodambaka, V. Petrova, S.V. Khare, D.D. Johnson, I. Petrov, and J.E. Greene, Phys. Rev. Lett. **88**, 146101 (2002).

²¹S. Kodambaka, S.V. Khare, V. Petrova, A. Vaillionis, I. Petrov, and J.E. Greene, Surf. Sci. **513**, 468 (2002).

²²J.J. Métois and J.C. Heyraud, J. Cryst. Growth **57**, 487 (1982).

²³G. Rao, D.B. Zhang, and P. Wynblatt, Acta Metall. Mater. **41**, 3331 (1993).

²⁴S. Surnev, P. Coenen, B. Voigtländer, H.P. Bonzel, and P. Wynblatt, Phys. Rev. B **56**, 12 131 (1997).

²⁵S. Surnev, K. Arenhold, P. Coenen, B. Voigtländer, H.P. Bonzel, and P. Wynblatt, J. Vac. Sci. Technol. A **16**, 1059 (1998).

²⁶K. Thürmer, J.E. Reutt-Robey, E.D. Williams, M. Uwaha, A. Emundts, and H.P. Bonzel, Phys. Rev. Lett. **87**, 186102 (2001).

²⁷A. Emundts, H.P. Bonzel, P. Wynblatt, K. Thürmer, J. Reutt-Robey, and E.D. Williams, Surf. Sci. **481**, 13 (2001).

²⁸Th. Michely and G. Comsa, Surf. Sci. **256**, 217 (1991).

²⁹K. Arenhold, S. Surnev, P. Coenen, H.P. Bonzel, and P. Wynblatt, Surf. Sci. **417**, L1160 (1998).

³⁰V.A. Shneidman and R.K.P. Zia, Phys. Rev. B **63**, 085410 (2001).

³¹P. Nozières, in *Solids Far From Equilibrium*, edited by C. Godrèche (Cambridge University Press, Cambridge, 1992), pp. 1–154.

³²C. Rottman and M. Wortis, Phys. Rev. B **24**, 6274 (1981).

³³J.E. Avron, H. van Beijeren, L.S. Schulman, and R.K.P. Zia, J. Phys. A **15**, L81 (1982).

³⁴E.D. Williams, R.J. Phaneuf, J. Wei, N.C. Bartelt, and T.L. Einstein, Surf. Sci. **294**, 219 (1993), **310**, 451(E) (1994).

³⁵L. Dobrzynski and J. Friedel, Surf. Sci. **12**, 469 (1968).

³⁶G. Tréglia and M.-C. Desjonquères, J. Phys. (France) **46**, 987 (1985).

- ³⁷A. Kara, S. Durukanoglu, and T.S. Rahman, Phys. Rev. B **53**, 15 489 (1996).
- ³⁸A. Kara, S. Durukanoglu, and T.S. Rahman, J. Chem. Phys. **106**, 2031 (1997).
- ³⁹S. Durukanoglu, A. Kara, and T.S. Rahman, Phys. Rev. B **55**, 13 894 (1997).
- ⁴⁰J.W.M. Frenken and P. Stoltze, Phys. Rev. Lett. **82**, 3500 (1999).
- ⁴¹H.J.W. Zandvliet, O. Gurlu, and B. Poelsema, Phys. Rev. B **64**, 073402 (2001).
- ⁴²P.J. Feibelman, Phys. Rev. B **62**, 17 020 (2000).
- ⁴³N. Akutsu and Y. Akutsu, J. Phys.: Condens. Matter **11**, 6635 (1999).
- ⁴⁴A. Emundts, Ph.D. thesis, RWTH Aachen, Germany, 2001.
- ⁴⁵H.S. Lim, C.K. Ong, and F. Ercolessi, Surf. Sci. **269/270**, 1109 (1992).
- ⁴⁶P. Wynblatt and H. P. Bonzel (unpublished).
- ⁴⁷R.C. Nelson, T.L. Einstein, S.V. Khare, and P.J. Rous, Surf. Sci. **295**, 462 (1993).